Stretch-Induced Stiffness Enhancement of Graphene Grown by Chemical Vapor Deposition
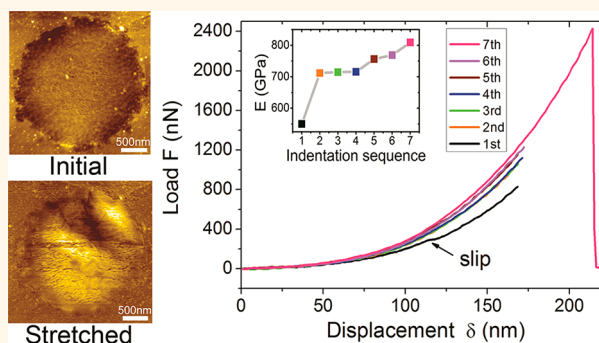
Qing-Yuan Lin,[†] Guangyin Jing,[‡,*] Yang-Bo Zhou,[†] Yi-Fan Wang,[†] Jie Meng,[†] Ya-Qing Bie,[†] Da-Peng Yu,[†] and Zhi-Min Liao[†,*]

[†]State Key Laboratory for Mesoscopic Physics, Department of Physics, Peking University, Beijing 100871, People's Republic of China and [‡]Department of Physics, Northwest University, Xi'an 710069, People's Republic of China

ABSTRACT The mechanical properties of ultrathin membranes have attracted considerable attention recently. Nanoindentation based on atomic force microscopy is commonly employed to study mechanical properties. We find that the data processing procedures in previous studies are nice approximations, but it is difficult for them to illustrate the mechanical properties precisely. Accordingly, we develop a revised numerical method to describe the force curve properly, by which the intrinsic mechanical properties of these membranes can be acquired. Combining the nanoindentation measurements with the revised numerical method, we demonstrate that loading−unloading cycles under large

load can lead to a pronounced improvement in stiffness of graphene grown by chemical vapor deposition (CVD). The Young's moduli of the stretched CVD graphene membranes can be improved to ∼1 TPa, closing to the value of the pristine graphene. Our findings demonstrate a possible way to recover the exceptional elastic properties of CVD graphene from the softened stiffness caused by wrinkles.

KEYWORDS: AFM · nanoindentation · zero-displacement point · wrinkle · Young's modulus

Recently, two-dimensional (2D) layered materials have attracted great interest for their intriguing properties. The 2D thin membranes such as graphene,[1,2] Bi_2Se_3,[3] and MoS_2[4] have been fabricated *via* various methods including mechanical exfoliation from bulk materials,[5] chemical vapor deposition (CVD),[6] and molecular beam epitaxial.[7] Many novel properties of the 2D membranes have been accordingly demonstrated. Particularly, the mechanical properties are primarily important to the fabrication of reliable functional devices and thus have attracted extensive attention.[8−12] Nanoindentation measurements performed by atomic force microscopy (AFM) have been widely used to acquire the elastic and fracture properties of nanomaterials such as carbon nanotubes,[13,14] silicon nanobeams,[15] gold nanowires,[16] ZnO nanobelts,[17] *etc.*, due to its ultrahigh spatial resolution and down to the piconewton force level.[18] Lee *et al.* first introduced this technique to measure the intrinsic

properties of mechanical exfoliated graphene.[8] The mechanical properties of the CVD graphene membranes[9] and monolayer MoS_2[12] have also been investigated using the similar nanoindentation method. Although this method has been widely employed to study the mechanical properties of ultrathin membranes, the reliability of the data processing procedure has never been discussed quantitatively. As reported by Lee[8] *et al.*, a nonlinear force-displacement dependence was proposed to derive the Young's modulus. To fit the force-displacement curve, the zero-displacement point (ZDP) needs to be determined in advance approximately.[8,19] However, the approximate determination of the ZDP may cause additional uncertainty for the analysis of the nonlinear force-displacement curve. On the other hand, previous indentation measurements of CVD graphene show that wrinkles can effectively soften the in-plain stiffness of graphene, and the existence of grain boundaries and voids leads to a

significant decrease of breaking strength.[9] Therefore, the growth of high quality graphene with large grain size[20] and exaltation of its stiffness are crucial for its mechanical applications.

Here we report that different selections of ZDP can significantly affect the yielded Young's moduli of CVD graphene membranes using the nanoindentation method, and thus it is particularly important to determine the ZDP precisely. Accordingly, we develop a modified numerical analysis method, which can determine the ZDP precisely and reveal the intrinsic properties of the membrane properly. Combining the nanoindentation measurements with the revised numerical method, we demonstrate a pronounced improvement in stiffness of CVD graphene by stretching the membrane with the AFM tip in repeating displacement controlled loading–unloading cycles. The maximum Young's modulus of the stretched CVD graphene can be improved to ∼1 TPa, which is comparable to the value measured from the pristine graphene membrane by Lee et al.[8] An increase of the surface area of the suspended membrane after stretching is also found, which may be ascribed to the flattening of wrinkles and thus resulting in the improvement of stiffness. Our results demonstrate a possible method to recover the exceptional elastic properties of CVD graphene from the softened stiffness caused by wrinkles.

RESULTS AND DISCUSSION

Large area uniform monolayer CVD graphene was grown on a copper foil[6] and transferred onto a silicon substrate[21] with arrays of circular holes to create free-standing graphene membranes. Figure 1a shows the topography image of a typical suspended membrane measured by AFM. Figure 1b is a scanning electron microscope (SEM) image of the transferred graphene, which verifies a relatively high yield of the graphene membranes on the holes. Raman spectroscopy was used to confirm that the CVD graphene was the nature of monolayer and with low defects,[22] as shown in Figure 1c.

For each suspended graphene membrane, the topography image was first acquired by the tapping mode of AFM. Then the center of the membrane was closely located right beneath the tip by zooming in, followed by the vertical loading with the tip.[8] Schematic diagram of the nanoindentation method is shown in Figure 2. The f–Z curves of the membrane were recorded, where f is the measured force and Z is the vertical position of the tip relative to the substrate. Details of the force curve measurement and data processing are discussed in the Materials and Methods section. Note that here the deflection of the membrane is denoted as δ, as shown in Figure 2.

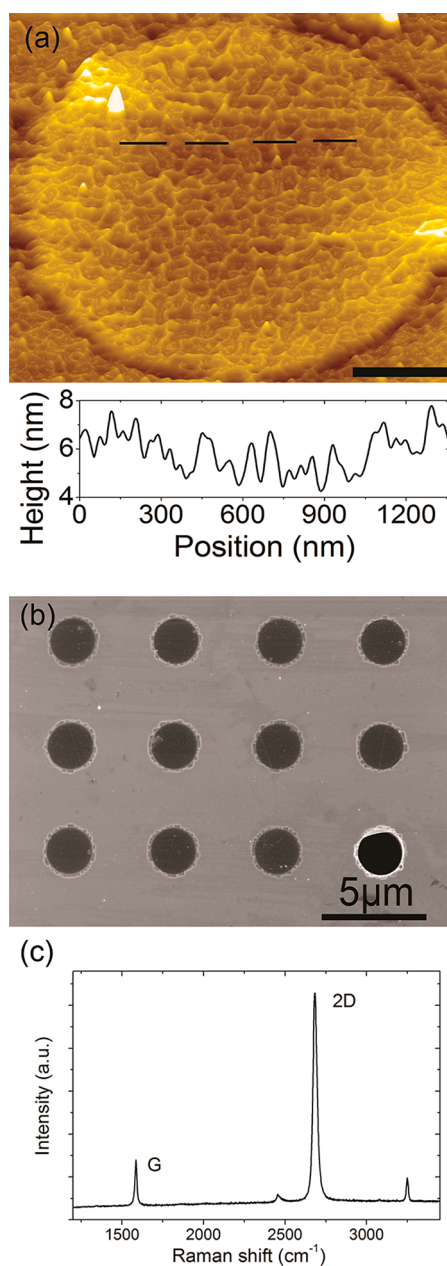The monolayer graphene suspended above a circular hole can be considered as an isotropic elastic

Figure 1. (a) AFM image and line profile on the dashed line of a suspended monolayer CVD graphene membrane. The hole is 2.2 μm in diameter (scale bar, 500 nm). (b) SEM image of the transferred graphene membranes. The dark hole represents the broken membrane. (c) Raman spectrum of one suspended monolayer graphene membrane. The D peak is almost invisible, indicating relatively low defect content.

membrane, and is firmly attached to the substrate along its perimeter and thus is treated as a clamped membrane with pretension. When a point load is applied at the center of the hole, the force-displacement curve of the membrane can be described as[8]

$$F = (\sigma_0^{2D}\pi)\delta + \left(\frac{E^{2D}q^3}{a^2}\right)\delta^3 \qquad (1)$$

where F and δ are the point load and the displacement of the membrane at the center, respectively, σ_0^{2D} is the

prestress, $E^{2D} = E \cdot h$ is the 2D Young's modulus with the thickness of h, $q = 1/(1.05 - 0.15\nu - 0.16\nu^2)$ is a constant where ν is the Poisson's ratio of the membrane, and a is the radius of the hole. In our measurement of CVD graphene, we take $h = 0.335$ nm, $q = 1.02$,[8] and $a \approx 1.1$ μm.

To use eq 1 to fit the data, a determination of the actual value of the load F and displacement δ according to the f–Z curve measured by AFM is needed.[23] During the AFM tip approaching process, the tip will be pulled downward to the sample slightly due to van der Waals interaction.[24] At the starting line, the measured
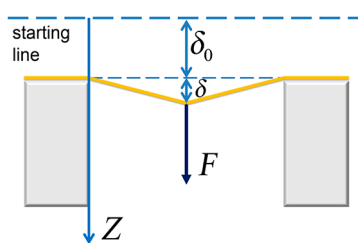

Figure 2. Schematic diagram of the nanoindentation method. During an indentation, the sample stage moves up to make the membrane contact with the tip, and the AFM cantilever is deflected upward to apply the downward load F on the membrane. Z is the vertical position of the tip relative to the substrate. The place of the tip where it has largest distance with the sample is defined as the starting line, where $Z = 0$. The distance between the starting line and the membrane is δ_0, and δ represents the displacement of the membrane.

force f is defined as zero, but the real force applied on the tip is actually not zero due to the tip–sample interaction. Therefore, the zero-displacement point, where δ and F should be zero, has to be determined in advance. The ZDP actually corresponds to a value of the measured force f_0 and the associated vertical position of the tip δ_0 on f–Z curve. Lee *et al.* had noticed this problem and developed a method to determine the ZDP.[8] After the tip makes contact with the sample, the force–time curve shows a linear behavior at very early stage, and Lee *et al.* assumed that the middle point of the linear part was the ZDP. The tip was first bent downward to make contact with the sample and later bent upward to apply a point load,[24] therefore the ZDP should be within this part. This method is a nice approximation for determination of the ZDP, but is not able to decide the ZDP precisely. Besides, as shown in their results, the unavoidable scattering of data makes it difficult to decide which part should be defined as the linear part, which also affects the determination of the middle point. We estimated that the ZDP will have an uncertainty of several nanometers in their method, which we find can greatly affect the yielded Young's modulus.

We then quantitatively discuss how the selection of the ZDP will affect the mechanical properties. We first performed indentation measurements on a suspended CVD graphene membrane and acquired a typical f–Z curve, as shown in Figure 3a. The red data points in the
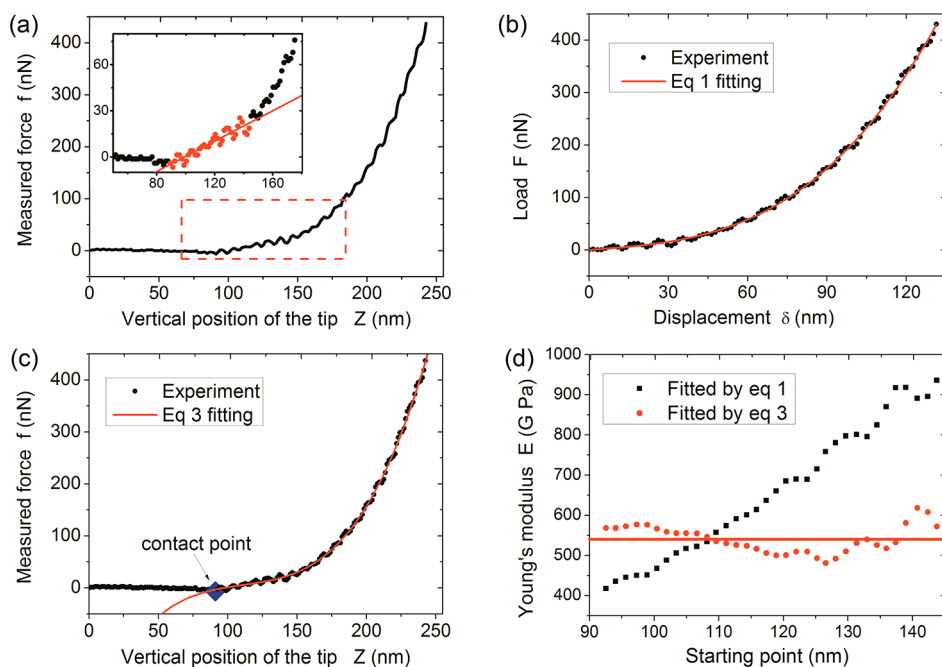

Figure 3. (a) A typical curve of force *versus* vertical position of the tip measured in a nanoindentation. Inset: red spots represent all the data points in the initial linear regime. (b) Selecting one point in the linear part as ZDP to form the curve of load *versus* displacement. Red line is the fitting according to eq 1. (c) The f–Z curve is fitted by eq 3 directly using the data acquired after the tip made contact with the membrane. (d) Comparison of the yielded Young's modulus by fitting the same part of data from the f–Z curve using eq 1 (black square) and eq 3 (red circle). The horizontal axis represents the Z value of the starting point of the selected data used for fitting. The red line $E = 540$ GPa represents the mean value of all the yielded Young's moduli fitted by eq 3.

inset of Figure 3a represent the linear part. We chose each data point of the linear part as the ZDP to fit the data using eq 1 to show how the different selections of ZDP affect the yielded Young's modulus. Figure 3b shows a typical $F-Z$ curve obtained by selecting one point in the linear part as ZDP and the fitting of the experiment data by eq 1. The results are shown as black squares in Figure 3d. The horizontal axis of Figure 3d represents the Z value of the selected ZDP and the vertical axis represents the yielded Young's modulus of the fitting. The Young's moduli range from 417 to 935 GPa. Note that all the Young's moduli were deduced from the same raw data. The result indicates that the Young's modulus is extremely sensitive to the selection of the ZDP in this method. Only 1 nm change in the vertical position of the selected ZDP will lead to ~10 GPa difference in yielded Young's modulus. As shown in Figure 3d, the ±25 nm uncertainty of the ZDP selection leads to *ca.* ±20% uncertainty in deflection, and the Young's modulus would have *ca.* ±60% uncertainty. The possible reason for such a result is that a small uncertainty of deflection would lead to tripled amount of uncertainty in Young's modulus according to the cubic term in eq 1.

To solve this problem, we developed a revised numerical method to determine the ZDP precisely. If the force f_0 and position δ_0 of the ZDP are treated as the unknown parameters of the $f-Z$ curve, eq 1 is rewritten as

$$f - f_0 = k_1(Z - \delta_0) + k_2(Z - \delta_0)^3 \qquad (2)$$

where $k_1 = \sigma_0^{2D}\pi$, $k_2 = E^{2D}q^3/a^2$ and $\delta = Z - \delta_0$, $F = f - f_0$. Then the part of $f-Z$ curve which was gathered after the tip makes contact with the sample can be described as

$$f = (f_0 - k_1\delta_0 - k_2\delta_0^3) + (k_1 + 3k_2\delta_0^2)Z - (3k_2\delta_0)Z^2 + k_2Z^3 \qquad (3)$$

Taking f_0, k_1, k_2, and δ_0 as free parameters, fitting the $f-Z$ curve using eq 3 gives precise values of f_0 and δ_0, and obtains the ZDP accurately. The prestress σ_0^{2D} and two-dimensional Young's modulus E^{2D} are directly calculated from the fitted values of k_1, k_2. Figure 3c shows the fitting of the $f-Z$ curve according to the eq 3. The revised formula eq 3 fits nicely to the experiment data. In this revised method, rather than to select

the ZDP manually, the ZDP is deduced directly by fitting the curve using eq 3. Theoretically, all the data after the contact point should follow eq 3. To clarify whether a different selection of data points will affect the calculated Young's modulus using the modified method, each data point in the linear part of the $f-Z$ curve is selected as the starting point of data to fit using eq 3. The results are shown as red circles in Figure 3d, which indicate that the yielded Young's moduli is 540 ± 33 GPa with an uncertainty of only 6.3%. Obviously, our revised method is convenient and rigorous, since the ZDP is no longer needed to be selected prior to the fitting. Expendably, our method is also suitable to study the mechanical properties of various ultrathin membranes that exhibit nonlinear force-displacement curves.

On the basis of the proper description of the mechanical properties as discussed above, we will study the stretching behavior of CVD graphene in the next part. The softened elastic response of CVD graphene has already been observed,[9] where the CVD graphene membranes were loaded within 200 nN and broke at that load. Considering that such a load is relatively small, the mechanical properties of the CVD graphene under a large load are still not clear. In our experiments, we observed that some of our membranes were able to suffer a large load. Therefore, it is worth examining the stiffness of the membrane experiencing loading—unloading cycles with large strain. We first stretched the membrane for several times to the same displacement to see the mechanical response variation. If the membrane could sustain such strain, we then gradually increased the load until the membrane fractured, and recorded the fracture force. Data of 47 free-standing CVD graphene membranes were recorded using the nanoindentation method. Histograms of the mechanical properties of these membranes are shown in Figure 4. All the membranes can be roughly grouped into two kinds. The first kind is the relatively weak membrane, which fractured in the first or second indentation test under a small load. The weak membranes have low stiffness and small fracture force, represented by the first peak in Figure 4a and the left part of Figure 4c. Sometimes this kind of membrane fractured between two consecutive indentations, and no fracture force was recorded. The second kind of
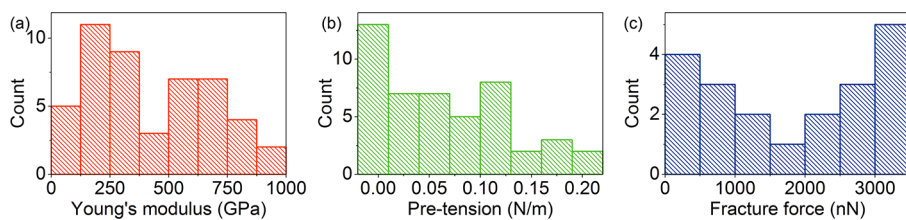

Figure 4. Histograms of (a) Young's modulus, (b) pretension, and (c) fracture force of the CVD graphene membranes. All the data were obtained by nanoindentation measurements of 47 membranes. The Young's modulus and pretension were calculated by fitting $f-Z$ curve using eq 3.

membrane can be repeatedly loaded. Most of the strong membranes fractured at a force of 2−3 μN. They have higher stiffness and a larger fracture force than those in the first kind, indicated by the second peak in Figure 4a and the right part of Figure 4c.

For the stronger membranes, we observed that by repeated stretching, the stiffness of the membrane can be enhanced. The Young's modulus of the membrane will gradually increase during consecutive indentations. Figure 5a shows a typical set of load *versus*
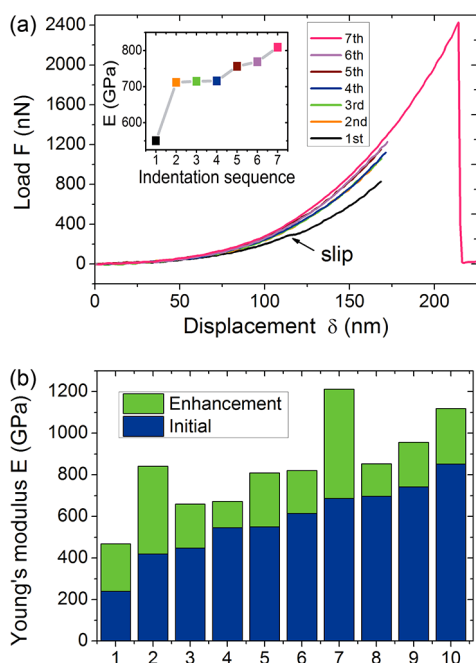

Figure 5. Improvement in the stiffness of the graphene membrane by stretching. (a) Seven consecutive load *versus* displacement curves of one membrane. A minor slip can be observed from the curve of first indentation. Inset shows the gradual increase of the Young's modulus. (b) Stiffness enhancement of 10 graphene membranes. Each column represents one membrane. The blue part is the initial Young's modulus of the membrane, and the green part is the enhancement amount after stretching.

displacement curves for a membrane, and the inset shows the gradual enhancement of the Young's modulus. The monolayer CVD graphene membrane was first repeatedly loaded for 6 times with the same displacement, and finally indented to fracture. For the first indentation, a slight slip occurred at the applied force of 290 nN. The yielded Young's modulus of this indentation was ∼550 GPa. After that, the second-fourth indentations showed a stiffer behavior, and the Young's moduli were all nearly 710 GPa. Next two indentations showed even stiffer response with a Young's modulus up to 750 GPa. Finally, we indented the membrane to failure, and this curve shows a Young's modulus of ∼800 GPa. For this membrane, ∼47% improvement in stiffness was observed. In all, 10 membranes in our experiments have shown such behavior, as shown in Figure 5b. A pronounced stiffness improvement of these membranes, ranging from 22% to 101%, suggested that stretching can improve the stiffness to a great extent.

To elucidate the mechanism of the stiffness enhancement and to directly detect how the membrane behaves after being stretched, we measured its morphology before and after indentation. We first measured the topography of a membrane, followed by stretching the membrane under a small load (∼100 nN) to confirm whether it could be repeatedly loaded or not. Then the topography after unloading was measured. Next, we repeatedly stretched the membrane by large load (∼1000 nN), and the stiffness enhancement of the membrane could be observed. At last we measured the topography to see the change in morphology after stretching. Figure 6 shows the morphology change of one typical membrane. Three pictures demonstrate the initial topography, topography after small load (∼100 nN), and topography after large load (∼1000 nN), respectively. Direct comparison of the line profile at the same place before and after indentation clearly shows the change in morphology
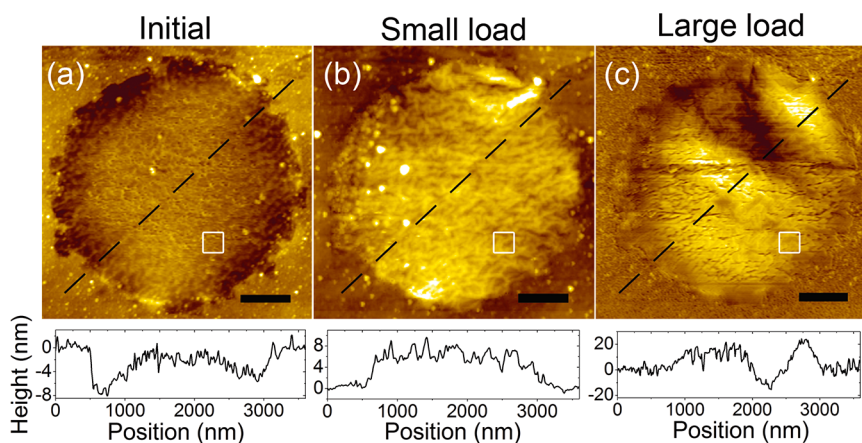

Figure 6. Morphology change of a typical membrane before and after indentation. The line profiles are extracted from the dashed lines in the AFM images. (a) Initial membrane. (b) Membrane measured after indentation cycles with small load. (c) Membrane after indentation cycles with large load. Scale bars, 500 nm.

(Supporting Information, Figure S4a). As shown in Figure 6, the origin membrane shows that the membrane adheres to the wall of the hole in the perimeter, and the middle part is relatively flat. The overall RMS roughness of this image with area of 2.5 × 2.5 μm^2 is 2.33 nm. After loading–unloading by small force, the membrane shows increased overall RMS roughness of 3.37 nm. Under large load, the morphology of the membrane changes greatly. The membrane exhibits a large fluctuation up to ~35 nm in amplitude and an overall RMS roughness of 6.86 nm. All the RMS roughness values were calculated according to the whole image. Previous experiments showed that nanoindentation will not cause sliding in the periphery.[8] By comparing the positions of small particles around the hole, we could not find any evidence of membrane sliding. Therefore, it can be concluded that the surface area of the suspended membrane was increased after stretching. Another tested membrane also showed similar behavior (Supporting Information, Figure S3). Nevertheless, the overall RMS roughness values represent the overall flatness of the images, but not the local surface roughness of the membrane. Therefore, we selected 150 × 150 nm^2 area to calculate the local surface roughness of the membranes, and the positions of these areas are marked by white squares in Figure 6. The local RMS roughness values of the selected area in the initial membrane, the membrane after small load, and the membrane after large load are 1.12, 1.04, and 0.95 nm, respectively. Without the influence of large fluctuations, the results demonstrated that the local surface roughness of the membrane was slightly reduced after stretching. The enlarged graphene surface area and reduced local surface roughness induced by loading–unloading cycles may suggest that the wrinkles of the membrane could be flattened due to large strain. As discussed by Ruiz-Vargas et al.,[9] for CVD graphene, unavoidable wrinkles will be introduced during growth and transfer procedures, and these wrinkles will soften the stiffness of graphene. Therefore, it is reasonable to ascribe the observed stiffness enhancement to the flattening of the wrinkles of the graphene membrane after stretching.

We also note that the membranes look almost buckled after larger indentations (Figure 6c and Supporting Information, Figure S3c). We believe that the buckling of graphene membranes after stretching does not contribute to the observed stiffness enhancement. The depression of the wrinkles under a large load led to the surface area enlargement of the membrane. After the tip detached from the membrane, the small residual stress of the membrane would spontaneously form the buckling due to the confinement of the boundary in the periphery, since the surface area of graphene is slightly larger than the hole. With the fact that such a structure is spontaneously formed due to small strain, the morphology could be easily changed with a small load. Previous simulations also indicate that warping will be suppressed by small initial elastic stretch.[25] Therefore, during nanoindentation, the buckling of the membrane will be flattened at the initial stage and will not affect the calculated stiffness of the membrane. Therefore, the strong buckling of the membrane plays a negligible role in the Young's modulus measurements.

CONCLUSIONS

We apply the nanoindentation method based on AFM to study the mechanical properties of CVD graphene, and find that it is particularly important to determine the zero-displacement point of the force-displacement curve precisely. We developed a modified numerical method to decide this point precisely, which allows us to investigate the intrinsic mechanical properties of the graphene membranes. This revised method may also be suitable for other ultrathin membranes that have similar mechanical properties with graphene. Stretching experiments of CVD graphene show that loading–unloading cycles could lead to an increase in the surface area of the suspended membrane, which may be attributed to the flattening of wrinkles. Our results therefore present a possible way to improve the stiffness of CVD graphene via loading–unloading cycles. This finding would be particularly helpful for designing nanodevices based on CVD graphene, such as large-scale graphene resonators.[26]

MATERIALS AND METHODS

Growth of CVD Graphene. Our monolayer graphene was grown using the CVD method,[6] on a 25 μm thick 99.8% copper foil in a tube furnace with CH_4 (35 sccm) and H_2 (2 sccm) as the sources, at a vacuum of 500 mTorr and at 985 °C for 20 min. During the growth process, the gas was continuously introduced to protect the sample until the temperature decreased to less than 100 °C.

Graphene Wet Transfer. Frist, a thin layer of poly-(methyl methacrylate) (PMMA) was spin-coated onto one side of the copper foil. The graphene on other side was then etched by air plasma with a flow rate of 15 sccm and power of 30 W for 10 s. Then the flake was floated in ferric chloride aqueous solution to etch away the copper foil. After rinsing the graphene/PMMA

film in deionized water for three times, the PMMA/graphene film was finally transferred onto the silicon substrate with arrays of circular holes fabricated by photolithography patterning followed by ICP-RIE etching. PMMA was later dissolved using acetone. Instead of directly pulling the samples out of acetone, we used a small box to take the substrate out of the acetone and put it into isopropyl alcohol, which allowed the substrate to be immersed in the solution during the procedure. This method nicely prevented further destruction due to the acetone surface tension while drying.[27]

Characterization. To measure the depth of the holes, the holes were half cut by focused ion beam. The diameter of ~2.2 μm and depth of ~5 μm of the holes were measured via SEM. After the graphene membranes were transferred on to the substrate,

we used SEM to confirm the coverage. Topography images of the free-standing membranes were measured in the tapping mode of AFM.

Force Curve Measurement and Data Processing. The force curves were measured by a scanning probe microscope system (SPI3800N, Seiko Instruments Inc., Japan). After the topography image was obtained, we changed the sample's XY position to locate the membrane's center right beneath the tip and performed nanoindentation measurement. We used nanosensors DT-NCLR-10 silicon cantilever with polycrystalline diamond coating to perform these nanoindentation measurements. The cantilever spring constant was 27 N/m, which was calibrated by the Sader method.[28] During an indentation, the sample moved up vertically to make contact with the tip and deflect the membrane according to the presetting upper/lower limits of z-piezo extension. In this procedure, only the change of the z-piezo extension and the change of cantilever deflection could be measured. The value of z-piezo extension and cantilever deflection at the starting line were automatically defined to be zero by the machine. Displacement controlled loading−unloading cycles were used to stretch the graphene membrane with the AFM tip. The measured force f was calculated by multiplying the cantilever deflection by the spring constant. A set of raw data of the measured force *versus* z-piezo extension were now available for further data processing. The value of Z was further obtained through subtracting the cantilever deflection from the z-piezo extension.[8] A f−Z curve was finally acquired. After the tip made contact with the membrane, the displacement of the membrane in the middle could be acquired from the change of Z value.

Conflict of Interest: The authors declare no competing financial interest.

Supporting Information Available: More details on sample fabrication, SEM image of the AFM probe, morphologies of another graphene membrane before/after indentation, further discussions on PMMA removal. This material is available free of charge *via* the Internet at http://pubs.acs.org.

REFERENCES AND NOTES

1. Novoselov, K. S.; Geim, A. K.; Morozov, S. V.; Jiang, D.; Zhang, Y.; Dubonos, S. V.; Grigorieva, I. V.; Firsov, A. A. Electric Field Fffect in Atomically Thin Carbon Films. *Science* **2004**, *306*, 666–669.
2. Novoselov, K. S.; Geim, A. K.; Morozov, S. V.; Jiang, D.; Katsnelson, M. I.; Grigorieva, I. V.; Dubonos, S. V.; Firsov, A. A. Two-Dimensional Gas of Massless Dirac Fermions in Graphene. *Nature* **2005**, *438*, 197–200.
3. Zhang, H. J.; Liu, C. X.; Qi, X. L.; Dai, X.; Fang, Z.; Zhang, S. C. Topological Insulators in Bi_2Se_3, Bi_2Te_3 and Sb_2Te_3 with a Single Dirac Cone on the Surface. *Nat. Phys.* **2009**, *5*, 438–442.
4. Mak, K. F.; Lee, C.; Hone, J.; Shan, J.; Heinz, T. F. Atomically Thin MoS_2: A New Direct-Gap Semiconductor. *Phys. Rev. Lett.* **2010**, *105*.
5. Novoselov, K. S.; Jiang, D.; Schedin, F.; Booth, T. J.; Khotkevich, V. V.; Morozov, S. V.; Geim, A. K. Two-Dimensional Atomic Crystals. *Proc. Natl. Acad. Sci. U.S.A.* **2005**, *102*, 10451–10453.
6. Li, X.; Cai, W.; An, J.; Kim, S.; Nah, J.; Yang, D.; Piner, R.; Velamakanni, A.; Jung, I.; Tutuc, E.; *et al.* Large-Area Synthesis of High-Quality and Uniform Graphene Films on Copper Foils. *Science* **2009**, *324*, 1312–1314.
7. Zhang, Y.; He, K.; Chang, C. Z.; Song, C. L.; Wang, L. L.; Chen, X.; Jia, J. F.; Fang, Z.; Dai, X.; Shan, W. Y.; *et al.* Crossover of the Three-dimensional Topological Insulator Bi_2Se_3 to the Two-Dimensional Limit. *Nat. Phys.* **2010**, *6*, 584–588.
8. Lee, C.; Wei, X.; Kysar, J. W.; Hone, J. Measurement of the Elastic Properties and Intrinsic Strength of Monolayer Graphene. *Science* **2008**, *321*, 385–388.
9. Ruiz-Vargas, C. S.; Zhuang, H. L.; Huang, P. Y.; van der Zande, A. M.; Garg, S.; McEuen, P. L.; Muller, D. A.; Hennig, R. G.; Park, J. Softened Elastic Response and Unzipping in Chemical Vapor Deposition Graphene Membranes. *Nano Lett.* **2011**, *11*, 2259–2263.
10. Suk, J. W.; Piner, R. D.; An, J. H.; Ruoff, R. S. Mechanical Properties of Monolayer Graphene Oxide. *ACS Nano* **2010**, *4*, 6557–6564.
11. Rafiee, M. A.; Rafiee, J.; Wang, Z.; Song, H. H.; Yu, Z. Z.; Koratkar, N. Enhanced Mechanical Properties of Nanocomposites at Low Graphene Content. *ACS Nano* **2009**, *3*, 3884–3890.
12. Bertolazzi, S.; Brivio, J.; Kis, A. Stretching and Breaking of Ultrathin MoS_2. *ACS Nano* **2011**, *5*, 9703–9709.
13. Salvetat, J. P.; Briggs, G. A. D.; Bonard, J. M.; Bacsa, R. R.; Kulik, A. J.; Stockli, T.; Burnham, N. A.; Forro, L. Elastic and Shear Moduli of Single-Walled Carbon Nanotube Ropes. *Phys. Rev. Lett.* **1999**, *82*, 944–947.
14. Salvetat, J. P.; Kulik, A. J.; Bonard, J. M.; Briggs, G. A. D.; Stockli, T.; Metenier, K.; Bonnamy, S.; Beguin, F.; Burnham, N. A.; Forro, L. Elastic Modulus of Ordered and Disordered Multiwalled Carbon Nanotubes. *Adv. Mater.* **1999**, *11*, 161–165.
15. San Paulo, A.; Bokor, J.; Howe, R. T.; He, R.; Yang, P.; Gao, D.; Carraro, C.; Maboudian, R. Mechanical Elasticity of Single and Double Clamped Silicon Nanobeams Fabricated by the Vapor−Liquid−Solid Method. *Appl. Phys. Lett.* **2005**, *87*.
16. Wu, B.; Heidelberg, A.; Boland, J. J. Mechanical Properties of Ultrahigh-Strength Gold Nanowires. *Nat. Mater.* **2005**, *4*, 525–529.
17. Ni, H.; Li, X. D. Young's Modulus of ZnO Nanobelts Measured Using Atomic Force Microscopy and Nanoindentation Techniques. *Nanotechnology* **2006**, *17*, 3591–3597.
18. Liang, J.; Fernandez, J. M. Mechanochemistry: One Bond at a Time. *ACS Nano* **2009**, *3*, 1628–1645.
19. Tombler, T. W.; Zhou, C. W.; Alexseyev, L.; Kong, J.; Dai, H. J.; Lei, L.; Jayanthi, C. S.; Tang, M. J.; Wu, S. Y. Reversible Electromechanical Characteristics of Carbon Nanotubes under Local-Probe Manipulation. *Nature* **2000**, *405*, 769–772.
20. Petrone, N.; Dean, C. R.; Meric, I.; van der Zande, A. M.; Huang, P. Y.; Wang, L.; Muller, D.; Shepard, K. L.; Hone, J. Chemical Vapor Deposition-Derived Graphene with Electrical Performance of Exfoliated Graphene. *Nano Lett.* **2012**, *12*, 2751–2756.
21. Li, X. S.; Zhu, Y. W.; Cai, W. W.; Borysiak, M.; Han, B. Y.; Chen, D.; Piner, R. D.; Colombo, L.; Ruoff, R. S. Transfer of Large-Area Graphene Films for High-Performance Transparent Conductive Electrodes. *Nano Lett.* **2009**, *9*, 4359–4363.
22. Ferrari, A. C.; Meyer, J. C.; Scardaci, V.; Casiraghi, C.; Lazzeri, M.; Mauri, F.; Piscanec, S.; Jiang, D.; Novoselov, K. S.; Roth, S., *et al.* Raman Spectrum of Graphene and Graphene Layers. *Phys. Rev. Lett.* **2006**, *97*.
23. Butt, H.-J.; Cappella, B.; Kappl, M. Force Measurements with the Atomic Force Microscope: Technique, Interpretation and Applications. *Surf. Sci. Rep.* **2005**, *59*, 1–152.
24. Cappella, B.; Baschieri, P.; Frediani, C.; Miccoli, P.; Ascoli, C. Force−Distance Curves by AFM. A Powerful Technique for Studying Surface Interactions. *IEEE Eng. Med. Biol. Mag.* **1997**, *16*, 58–65.
25. Wei, Y.; Wu, J.; Yin, H.; Shi, X.; Yang, R.; Dresselhaus, M. S. The Nature of Strength Enhancement and Weakening by Pentagon−Heptagon Defects in Graphene. *Nat. Mater.* **2012**, *11*, 759–763.
26. van der Zande, A. M.; Barton, R. A.; Alden, J. S.; Ruiz-Vargas, C. S.; Whitney, W. S.; Pham, P. H. Q.; Park, J.; Parpia, J. M.; Craighead, H. G.; McEuen, P. L. Large-Scale Arrays of Single-Layer Graphene Resonators. *Nano Lett.* **2010**, *10*, 4869–4873.
27. Song, L.; Qing, Z.; Jun, X.; Kai, Y.; Hailin, P.; Fuhua, Y.; Liping, Y.; Dapeng, Y. Fast and Controllable Fabrication of Suspended Graphene Nanopore Devices. *Nanotechnology* **2012**, *23*, 085301.
28. Sader, J. E.; Chon, J. W. M.; Mulvaney, P. Calibration of Rectangular Atomic Force Microscope Cantilevers. *Rev. Sci. Instrum.* **1999**, *70*, 3967.